Optical filters for stereoscopic image sensors

M. J. Maciel, M. F. Silva, R. P. Rocha, J. P. Carmo, J. M. Gomes, and J. H. Correia
University of Minho, Dept. Industrial Electronics, Guimarães, Portugal
jcarmo@dei.uminho.pt

***Abstract*—This paper presents optical filters for integration on stereoscopic image sensors. The filters must cover each one of primary colors within the visible, in order to yield a passband around the respective wavelengths. Dielectric materials based on SiO_2 and TiO_2 were used due to their compatibility with silicon. The best simulation with only 3 dielectric layers resulted in optical filters with full width at half maximum (FWHMs) of 79, 95 and 124 nm and central wavelengths of 456, 529 and 605 nm, respectively.**

Keywords—Modeling and simulation, optical filters, RGB, image sensor, microlenses, stereoscopy.

I. INTRODUCTION

In the present days, the range of applications based on optics is wide and don't cease to increase [1-9]. Examples of applications include optical sensors, optical sources, laser sources, lighting, optical communications, image sensors, displays, solar cells and so on [8]. Under normal circumstances, an optical sensor requires optical filters with a large number of layers either for providing a sharp transition between the pass and the stop-band or for providing pass-bands with a very small width. Fortunately, the human eye can't distinguish between well-confined pass-bands with sharp transitions to the stop-band and not so well defined pass-bands with smoothed transitions to the stop-band. In this context and taking into account the need to reduce their complexity for decreasing the costs and at the same time optimizing the time required on their fabrication, it was put an effort to design optical filters with the smallest possible number of layers. For this reason, the optical filters presented in this paper were designed with only three dielectric layers for a reasonable coverage of each one of primary colors (red, green and blue - RGB) and to yield a passband around the respective wavelengths.

II. DESIGN

The optical filters presented in this paper were designed for integration into optical microsystems for allowing the acquisition of polychromatic stereoscopic images. Figure 1 illustrates the architecture of the targeted image sensor, which is composed by two pupils (two entrance apertures just like the human eyes) from where both the left and right images (that originate the tridimensional effect) pass through before being focused into the photodetectors by an objective lens. This lens focuses the two incident beams in the direction of an array of microlenses. Then, the light is concentrated into the photodetectores, which defines a small sensitive area where the light is converted to currents and further amplified and used by a display device. The photodetectors are based on CMOS photodiodes, where the left and right images are separated by focusing each side onto the appropriate sensor column under the microlens, whose fabrication on top of the optical filters is desired. For this reason, the optical filters are the focus of analysis in this paper.

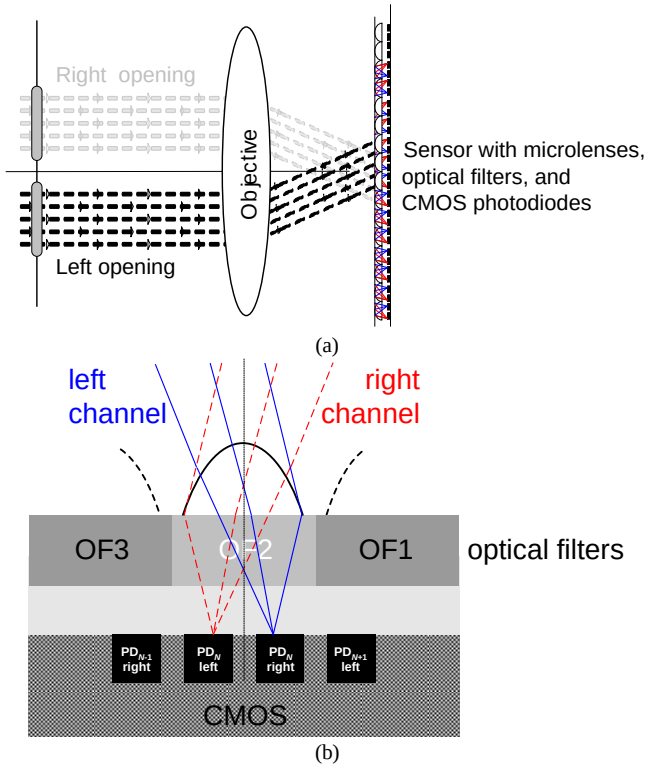

Fig. 1. Illustration of the stereoscopic image formation, and (b) illustration of the concept associated to the microlenses array for stereoscopic acquisition with a single polychromatic CMOS image sensor (example with one lens and two photodiodes PD_N left and right).

As illustrated in Figure 2, microsystem integration require layers of two different dielectric materials. These dielectric materials are selected in order to make their indexes of refractions being different with relation to each other. The example of Figure 2 helps to illustrate the mechanism that explains the wavelength filtration. The reflected light is the combination of four k reflected beam with four different phases and amplitudes, where each component k contains its own optical path d_k. The same applies to the transmitted light, which is simply given by the difference between the incident and the reflected light. If A_0 is the amplitude of the incident light, then each k reflected component will be $A_0.A_k.\exp(-j\beta_k.d_k)$, with $|A_k|<1$ and $\beta_k=2\pi/\lambda_k$. This makes both the reflected and the transmitted light wavelength λ dependent. This interferometer-based mechanism is what explains the optical filtration with respect to the wavelength.

978-1-4799-0518-8/13/$31.00 ©2013 IEEE

The fabrication technology of the optical filters must allow their integration with the microelectronics (comprising photodetectors and respective readout electronics) on post-processing steps. This can be easily achieved with dielectric materials compatible with the silicon. Examples of dielectric materials extensively used on microsystems due to their compatibility with silicon are: silicon dioxide (SiO_2), titanium dioxide (TiO_2) and silicon nitride (SiN), whose typical indexes of refractions are respectively, 1.5, 3 and 2.16.

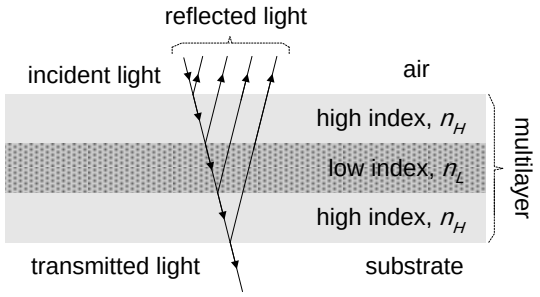

Fig. 2. A multilayer consisting of alternate high and low index of refraction.

The selected materials for fabricating the optical filters were the TiO_2 and the SiO_2 because the same reactive RF sputtering thin-films deposition technique can be used. Additionally, it is extremely difficult or even impossible to remove these materials from the silicon substrate. Moreover, the index of refraction of the SiO_2 is almost constant in the visible range (e.g. between 400 and 740 nm). The TiO_2 was also selected due to fabrication constraints (the deposition process is well characterized) and because it is compatible with the silicon that forms the microelectronic circuits. This last issue is very important because this material is the first one to be deposited. Finally, the TiO_2 and the SiO_2 where also selected because all depositions can be done without open the deposition chamber, thus avoiding air contamination and temperature gradients.

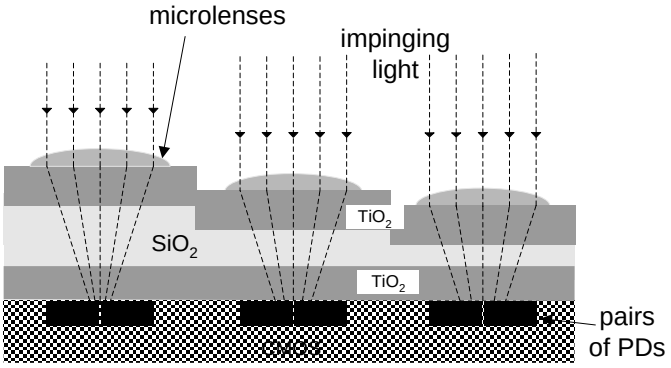

Fig. 3. Illustration of the 3 optical filters with 3 dielectric layers (each one composed by a sequence of *HLH* materials. It must be observed that the thickness of the inner layer (where the *L* material is deposited) is not the same for the 3 filters, in order to create 3 top-to-bottom wavelenght pass-bands.

The optical filters will be postprocessed by reactive plasma sputtering deposition of thin-films on top of the photodetectors. The filter fabrication starts with the deposition of a TiO_2 layer after the completion of the standard CMOS process, including the removal overlayer (this issue will be further discussed). Then, the subsequent layers of SiO_2 and TiO_2 will be deposited with the suitable thicknesses. Figure 3 illustrates a cut view with the structure the optical filters, where it can be observed the existence of three layers. The middle layer of the filters is composed by SiO_2, e.g., it is filled with the material with smaller index of refraction, and for this reason is denominated by ***L***. Additionally, the external layers are composed by TiO_2 (the higher index of refraction, e.g., the ***H*** material). The thickness of the SiO_2 middle layer is what defines the central wavelength λ_i, $i \in \{\text{red}, \text{green}, \text{blue}\}$, whereas the up and bottom layers are the main responsible for defining the bandwidth.

Figure 4 shows the simulated transmittances [%] versus the wavelength [nm] in the visible range that were obtained with the three optical filters, whose characteristics are listed in the Table I. The simulations were performed using a freeware tool for thin-films calculations [10].

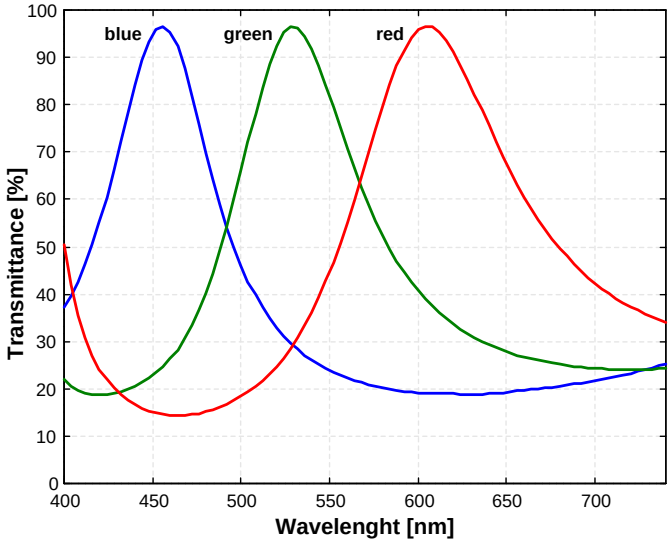

Fig. 4. Simulated transmittance for the 3 RGB optical filters.

Table I: Thicknesses of the 3 dielectric layers that form the optical filters illustrated in the Figure 3, whose simulated transmittances are in the Figure 4.

λ_0 [nm]	Layer number [#]		
	1	2	3
	Thickness [nm]		
blue 456 nm	45	140	45
green 529 nm	45	180	45
red 605	45	220	45

Figure 4 also allows to observe that the best simulations with only three dielectric layers resulted in optical filters with full width at half maximum (FWHMs) of 124, 95 and 79 nm and central wavelengths of 605, 529 and 456 nm, e.g., in the red (R), green (G) and blue (G) regions of the visible spectrum, respectively. Moreover, the simulations seems to be promising

because the superposition of the three optical filters reasonably covers the entire visible spectrum (e.g., the 400-740 nm range).

III. EXPERIMENTAL

Few depositions of thin-films made of TiO_2 were performed on top of glass substrates in order to evaluate and demonstrating the suitability for fabricating arrays of microlenses above the optical filters. The other two depositions of SiO_2 and TiO_2 were not done because their total thickness didn't affect the reflow process. This fact can be twice explained by analyzing the thermal conductivities of these materials: TiO_2, SiO_2, glass and silicon materials which are respectively, 6.5, 1.3, 0.8 and 148 $W.m^{-1}K^{-1}$. First and for depositions on top of silicon, the two remain layers of SiO_2 and TiO_2 don't make difference because, when compared with SiO_2 and TiO_2, the dominant thermal effect is due to the high thermal conductivity of silicon. Second and for depositions on top of glass, the two remain layers of SiO_2 and TiO_2 don't also make difference because, when compared with SiO_2 and TiO_2, the glass substrate strongly affects the reflow due to both its larger thickness (1 mm) and small thermal conductivity (compared with those found on SiO_2 and TiO_2 thin-films). Therefore, only one thin-film was considered, e.g., the material that constitutes the top layer of the optical filters. In this context, the depositions were performed by the reactive RF sputtering technique. A reactive atmosphere composed by argon (Ar) and oxygen (O_2) was used during the depositions. In these depositions, the gas flows were maintained at 25 and 2 sccm of argon and oxygen, respectively.

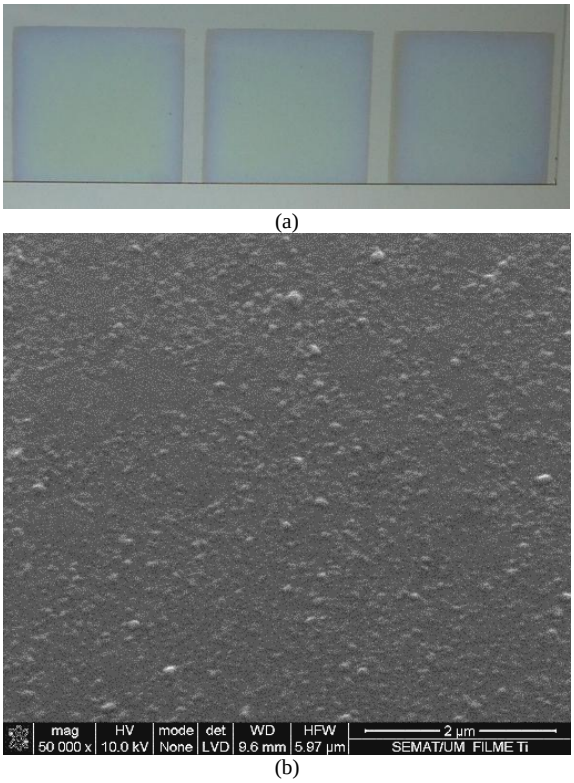

(a)

(b)

Fig. 5. (a) the photography and (b) the respective (top) SEM image of a selected sample of a thin-film made of TiO_2 before doing the deposition of the material that will be used in the fabrication of the microlenses array.

Figure 5 shows (a) the photography and (b) the respective (top) SEM image of a selected sample of a thin-film made of TiO_2 before depositing the material that will form the array of microlenses (e.g., the AZ4562 photoresist). A naked eye analysis of the SEM image reveals a thin-film whose surface shows a reasonable uniformity (low roughness). This issue is important for decreasing the stray-light effect and therefore, to avoid the degradation of the filter's characteristics (central wavelength and FWHM). Thin-films with good uniformity is also important for fabricating microlenses on top of their surface.

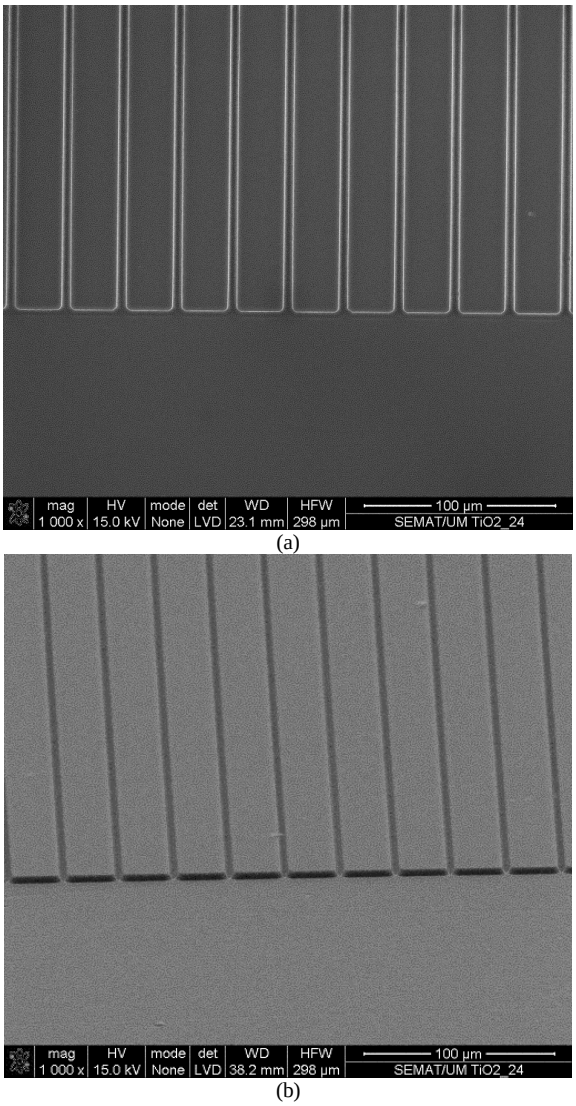

(a)

(b)

Fig. 6. Two SEMs showing the top view of few AZ4562 strips that were deposited on top of a thin-film made of TiO_2. These SEMs were acquired at two different angles for a better illustration purpose.

Few arrays of microlenses were fabricated on top of the titanium dioxide films. The AZ4562 photoresist was the selected material due to the fabrication requirements. The AZ4562 is a positive photoresist, which is ideal for coating thicknesses above 3-5 µm without having to increase the exposure energy considerably and still providing enough energy down to the substrate of the AZ. The SEM photographs

in Figure 6 refer to arrays of rectangular strips seen from the top, which after being reflowed will result on arrays of microlenses with an hemicylindrical shape. These arrays are constituted by AZ4592 photoresist. The two SEMs of the Figure 6 were obtained at two different angles on top of the AZ4562 strips' array for better illustrating their transparency and shape (e.g., high aspect ratio and tridimensionality). The SEM in Figure 7(a) shows a close-in zoom of the selected strip of AZ4562, whereas the SEM in Figure 7(b) shows the cross section of the selected AZ4562 strip.

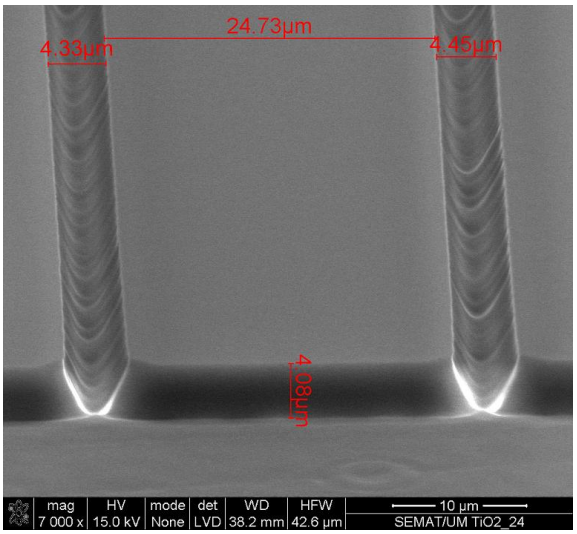

(a)

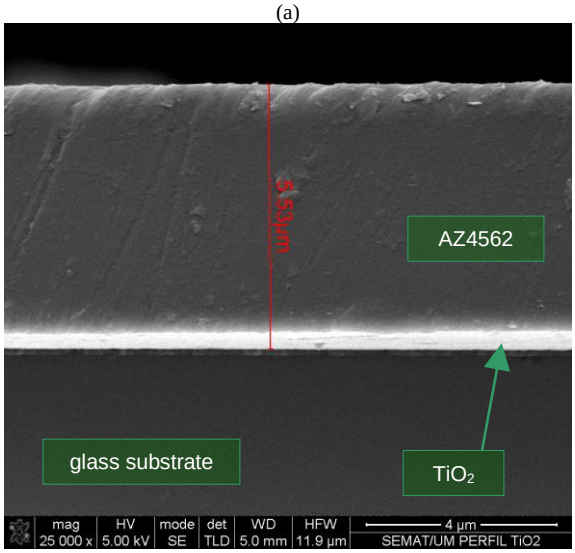

(b)

Fig. 7. (a) A SEM showing the close-in zoom of a selected AZ4562 strip; and (b) a SEM with the cross section of the selected AZ4562 strip.

IV. Conclusions

This paper presented the design of optical filters for integration with stereoscopic image sensors. The design was optimized for the minimum number of dielectric layers, in order to decrease the complexity of fabrication for achieving reduced costs. Only three dielectric layers are required thanks to the desired application that allow relaxed specifications, e.g., the perception sensed by the human brain is not sensitive to reasonable shifts in the pass-band spectrums of different colors. Therefore, precise central wavelengths and bandwidths are not required. Additionally, since the stereoscopic image sensor require arrays of microlenses, then few arrays of AZ4562 were deposited on top of the external layer of optical filters (made of TiO_2) in order to validate the suitability of the concept.

Acknowledgment

This work and the scholarships of MSc José Miguel Gomes and MSc Marino Jesus Maciel were fully supported by the Portuguese Foundation for Science and Technology (FCT) under the PTDC/EEA-ELC/109936/2009 project grant. MSc Rui Pedro Leitão Rocha was fully supported by the Doctoral scholarship SFRH/BD/33733/2009 also granted by the FCT in the scope of the LTI's Doctoral Program sponsored by MIT-Portugal. The authors are in debt with the PhD student Manuel Fernando Ribeiro da Silva for his support during the deposition of TiO_2 thin-films. The authors also acknowledge to Dr. Ing Christian Koch from the company MicroChemicals GmbH for the technical support.

References

[1] C. Shen, *et al.*, "Micromachined nanofiltration modules for lab-on-a-chip applications", Journal of Micromechanics and Microengineering, Vol. 22, pp. 1-10, 2012. Paper number 025003.

[2] M. Haurylau, *et al.*, "On-chip optical interconnect roadmap: challenges and critical directions", IEEE Journal of selected Topics in Quantum Electronics, Vol. 12, No. 6, pp. 1699-1706, 2006.

[3] J. S. Levy, *et al.*, "CMOS-compatible multiple-wavelength oscillator for on-chip optical interconnects", Nature Photonics, Vol. 4, pp. 37-40, 2010.

[4] M. Harmand, *et al.*, "Achieving few-femtosecond time-sorting at hard X-ray free-electron lasers", Nature Photonics, Vol. 7, pp. 215-218, 2013.

[5] R. Slavik, *et al.*, "All-optical phase and amplitude regenerator for next-generation telecommunications systems", Nature Photonics, Vol. 4, pp. 690-695, 2010.

[6] N. Horiuchi, "Nanowire arrays", Nature Photonics, Vol. 7, pg. 166, 2013.

[7] N. G. Horton, "*In vivo* three-photon microscopy of subcortical structures within an intact mouse brain", Nature Photonics, Vol. 7, pp. 205-209, 2013.

[8] R. A. Taylor, *et al.*, "Nanofluid-based optical filter optimization for PV/T systems", Light: Science & Applications, Vol. 1, 2012.

[9] S. Koyama, et *al.*"A day and night vision MOS imager with robust photonic-crystal-based RGB-and-IR", IEEE Transactions on Electron Devices, Vol. 55, No. 3, pp. 754-759, 2008.

[10] Fredrik Hansteen, Thinfilm v.1.2, Simulation tool. Available online in the web address: **`thinfilm.hansteen.net`**. Used on 18th March 2013.